Geophysical Journal International

Geophys. J. Int. (2013) **195,** 844–853
Advance Access publication 2013 August 16

doi: 10.1093/gji/ggt293

Geomagnetically induced currents in the Uruguayan high-voltage power grid

R. Caraballo,[1,2] L. Sánchez Bettucci[2,3] and G. Tancredi[4]

[1] *Facultad de Ingeniería, Universidad de la República, J. H. y Reissig* 565 CP 11300, *Montevideo, Uruguay. E-mail: jolinar35@gmail.com*
[2] *Observatorio Geofísico de Aiguá, Road* 39 *km* 60, *CP* 20500, *Maldonado, Uruguay*
[3] *Área Geofísica-Geotectónica, Instituto de Ciencias Geológicas, Facultad de Ciencias, Universidad de la República, Igua* 4225 CP 11400, *Montevideo, Uruguay*
[4] *Departamento de Astronomía, Instituto de Física, Facultad de Ciencias, Universidad de la República, Igua* 4225 *CP* 11400, *Montevideo, Uruguay*

Accepted 2013 July 18. Received 2013 July 11; in original form 2011 October 12

SUMMARY

We estimate the influence of the geomagnetically induced currents (GIC) on the Uruguayan electrical distribution grid. The GIC are related to time variations in the geomagnetic field caused by the interaction of the solar wind with the Earth's magnetosphere. These currents may cause several problems in power grids, pipelines, among others. South America is close to the South Atlantic Magnetic Anomaly (SAA). Particle precipitation in the anomaly region could lead to pulsations in the horizontal component of the geomagnetic field, that may contribute to the GIC production. Scarce research has been done to assess the space weather impact on this area.

Due to the lack of magnetic field data at the Uruguayan territory, spherical elementary currents system (SECS) was used to interpolate field values with data available from three magnetic observatories located at Vassouras, Trelew and São Martinho da Serra. The simple topology of the Uruguayan power grid provides some advantages in the calculation of GIC. To calculate these currents, a plane wave method combined with a ground conductivity model was used. Estimated GIC suggest peak currents *ca*. 15 A, at the earthing points of some substations in a 770 km power line during the Halloween Magnetic Storm on 2003 October 29.

Key words: Electromagnetic theory; Geomagnetic induction; Rapid time variations.

1 INTRODUCTION

Currently we are experiencing solar cycle 24 which thus far, seems to be quieter than the previous solar cycle 23. Despite this, the severe solar activity perturbs the Earth's magnetosphere driving huge amounts of charged particles into the radiation belts. These trapped particles, principally protons and electrons, impinge on the upper atmosphere creating auroras and ionospheric electrojets.

The geoelectric field induced by geomagnetic disturbances at the Earth's surface produces geomagnetically induced currents (GIC) in transmission lines and pipelines.

Space weather constitutes a major concern in scientific community due to their effects on technological infrastructure. As the extent of power networks grows up to reach continental scale, the electronic hardware attached becomes more sensitive to the effects of GIC.

There is a considerable amount of documentation related to the impact of geomagnetic activity on the Northern Hemisphere infrastructures (e.g. Kappenman 2007; Pirjola 2007). At mid-latitudes, the damages suffered in transformers at the South African power grid during the Halloween storm in 2003 October have been attributed to GIC effects (Bernhardi *et al.* 2008). However, in the area of the South Atlantic Anomaly (SAA), scarce research has been done to assess the space weather impact (Jayanthi *et al.* 1997; Trivedi *et al.* 2005).

Since 2011, a group of researchers concerned with this phenomenon have been mounting a geomagnetic station in the south east side of the Uruguayan territory. One of its aims is to study space weather and its effects on the Rio de la Plata area. The new magnetic observatory (Observatorio Geofísico de Aiguá, OGA) (Fig. 1) is located at (34.33°S, 54.71°W).

1.1 The SAA

Far from the Earth, the magnetic field behaves mainly as dipolar but, close to the surface, higher order field components and its eccentricity with respect to the Earth's centre become relevant. This is accepted to be the origin of the anomaly (Kivelson & Russell 1995). The SAA is a zone of weakened magnetic field intensity on the Earth with a total intensity *ca*. 23.000 nT (WMM 2010; Fig. 1), almost one third than the maximum magnetic field value. According to Trivedi *et al.* (2005) the centre of the anomaly lies near 26°S, 54°W, in southern Brazil. Geomagnetic field values registered in Uruguay

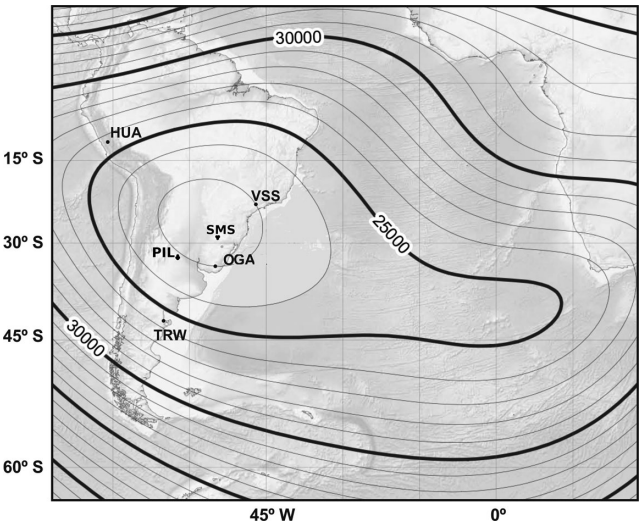

Figure 1. Intensity map depicting the contour line in 25 000 nT of the South Atlantic Anomaly (SAA) and the locations of the working magnetic observatories in the area. Vassouras (VSS), São Martinho da Serra (SMS), Aigua (OGA), Trelew (TRW), Pilar (PIL) and Huancayo (HUA). *Source*: http://ngdc.noaa.gov/geomag/WMM.

are close to 22.850 nT at OGA and decreases slightly towards the northern side of the country to values *ca.* 22 650 nT, suggesting a south western gradient. The SAA has been expanding and drifting westwards at a rate of 0.3° yr^{-1} (Kivelson & Russell 1995), close to the estimation for the differential rotation of the Earth's core and its surface. The weak magnetic field in the anomaly leads to a deeper penetration of energetic particles into the ionosphere.

Enhanced electron flux cause dielectric charge accumulation, memory upsets and failures in spacecrafts travelling into low orbits.

The electron precipitation occurring into the D and E layers of the ionosphere over the SAA has been correlated with Pc3-4 pulsations in the X-ray flux and the horizontal component of the geomagnetic field (**H**) (Jayanthi *et al.* 1997; Trivedi *et al.* 2005). Trivedi *et al.* (2005) found an enhancement of H impulsive amplitudes at a location close to the centre of the SAA, compared to another station further away, during a sudden storm commencement (SSC). They ascribe the enhancement due to electron precipitation in the SAA region.

1.2 Geomagnetically induced currents

The GIC are quasi-dc-like currents (1–0.001 Hz). Depending on their intensity, they can cause from small troubles to severe damages in HV transformers. GIC influence leads to half cycle saturation in the transformer's core, driving it into non-linear operation with the increase of the exciting current (Kappenman 2007). This implies harmonics generation, heavy reactive power demands, voltage drops and even blackouts. Although, power networks are designed to overcome weather effects, these effects are geographically localized. On the contrary, the GIC affects extensive areas in a large network quite simultaneously. This could yield to a massive failure in terms of minutes (Kappenman 2007). Other effects include perturbation on corrosion control in buried pipelines, among others. The intensity of GIC depends on the time variation of the geomagnetic field, the grid's topology and resistances.

In a similar way, the accuracy of the geoelectric field assessment is strongly dependent on the knowledge of the ground conductivity

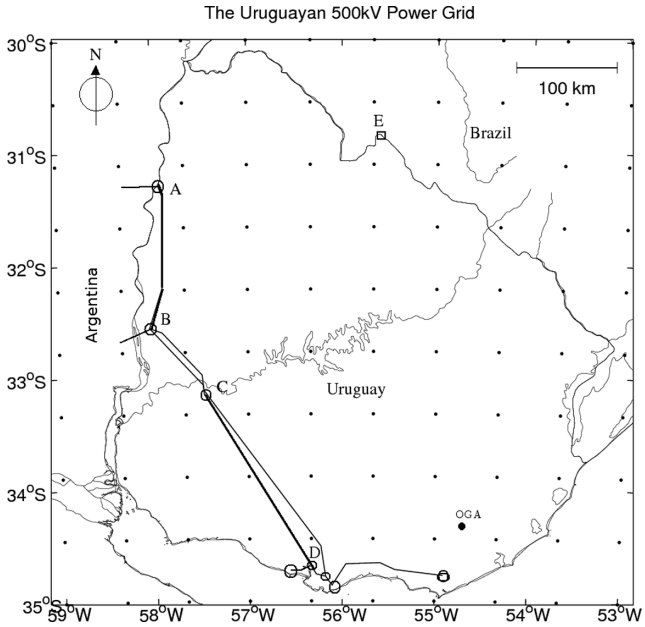

Figure 2. Uruguayan 500 kV power grid. The thick lines indicate the sections considered. (A) Salto Grande Dam, (B) San Javier, (C) Palmar Dam, (D) Montevideo (four substations), (E) Brazilian frequency converter substation. Circles denote HV substations, the dots show the interpolation points *Source*: Unidad Reguladora de Servicios de Energia y Agua URSEA. 2010.

structure (Pirjola 1982; Kappenman 2007), that is, less conductive soils are more prone to generate intense GIC.

1.3 Characteristics of the Uruguayan power grid

According to the Uruguayan office for water and energy management (URSEA), the present HV power grid in Uruguay is composed essentially by two main branches partially interconnected: a principal branch of ∼770 km aerial AC lines at 500 kV; the other one is composed by several sections of 350 km length at 150 kV. These branches were developed in a sort of parallel configuration.

The power grid is mainly north–south oriented, with some secondary branches in the East–West direction. The whole of the HV network carries three phase AC current. Nowadays, the Uruguayan grid is interconnected with the Argentinian network by the Salto Grande power station and San Javier substation. In the north, a frequency converting station connects the 150 kV network with the Brazilian network. Fig. 2 depicts the 500 kV power grid with the sections considered. This branch interconnects three power stations that supply *ca*. 70 per cent of the total generation. Failures in these power lines lead to blackouts over the most populated areas in the south of the country.

2 CALCULATION OF GEOMAGNETICALLY INDUCED CURRENTS

To calculate the GIC over a network, we can assume a plane electromagnetic wave penetrating into the ground. This is a two-step process (Pirjola 1982; Boteler & Pirjola 1998).

(i) Determination of the geoelectric field **E**, induced at the Earth's surface.

(ii) Calculation of the GIC produced by the **E**-field over the conducting network.

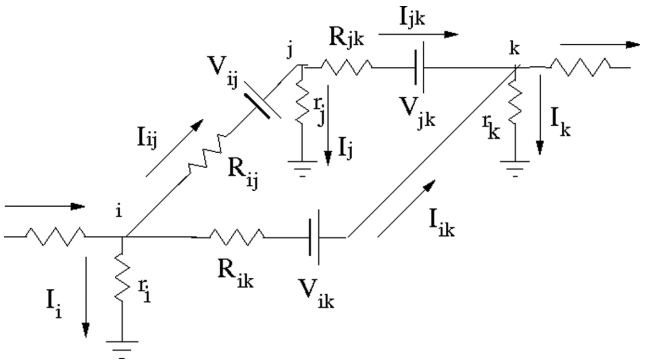

Figure 3. Modelling GIC as sources over the branches of a power network section. The resistances R_{ij} between i and j nodes represent the conductor's resistances. The $(i, j, k, \dots)$ nodes are earthed through $(r_i, r_j, r_k, \dots)$ resistances, respectively.

Two main issues involve the first step: the evaluation of the geomagnetic disturbances at each point of interest and the knowledge of ground conductivity structure.

Regarding to the second step, we cannot select an arbitrary zero point of the potential along the network. Then it is necessary to include voltage sources along some trajectories to represent the GIC influence as it is shown in Fig. 3 (Boteler & Pirjola 1998).

2.1 Geomagnetic field interpolation

Since the power grid considered is far away from the nearest magnetic observatory, it is necessary to interpolate the geomagnetic field variations at each node (Bernhardi *et al.* 2008). To overcome the lack of geomagnetic data for the event considered, spherical elementary current system (SECS) technique (Amm & Viljanen 1999) was used to interpolate field values along the Uruguayan territory.

SECS is an inversion method that uses observed geomagnetic data to infer equivalent ionospheric currents. These currents are not real, but mathematically reproduce the geomagnetic field observed at the Earth's surface. SECS has been used widely to calculate geomagnetic field components when the ionospheric contribution to the geomagnetic disturbance is important.

As GICs are a regional phenomenon, we can neglect the Earth's curvature and planar geometry can be used instead of the spherical one. In such a scheme, the horizontal magnetic field due to an elementary ionospheric current at height h, with amplitude I, in a cylindrical reference frame with axis at the pole of such current is given by:

$$\vec{B} = \frac{\mu_0 I}{2\pi r}\left(1 - \frac{h}{\sqrt{r^2 + h^2}}\right)\vec{e}_r, \tag{1}$$

where $r = \sqrt{x^2 + y^2}$ is the radial distance from the current element to the field point over the x,y-plane (i.e. the Earth's surface), $\vec{e}_r$ is the radial unit vector and μ_0 the vacuum permeability. Usually in geoelectromagnetics, Y denotes the **B** component to the eastward direction and X refers to the northward component. In practice, these horizontal components are sufficient to perform the calculation.

Let M elementary currents I, be placed freely over the interest area to improve the accuracy. Such currents are calculated by fitting the modelled geomagnetic disturbance to the observed one at N particular locations. Usually this system is underdetermined ($N < M$), giving a set of equations as:

$$\mathbf{B} = \mathbf{TI}, \tag{2}$$

where the elements of the $N \times 1$ matrix **B**, $B(x_j, y_j)$ $(j = 1, \dots, N)$, represent the components observed at N points on the surface. **T** is an $N \times M$ matrix whose elements are defined by:

$$T_{ij} = \frac{\mu_0}{2\pi r}\left(1 - \frac{h}{\sqrt{r^2 + h^2}}\right),\ i = 1, \dots, N;\ j = 1, \dots, M, \tag{3}$$

represent geometrical factors calculated at the points (x_i, y_i) on the Earth's surface due to an elementary unit amplitude current element located at (x_j, y_j), and height $h = 100$ km in the ionosphere (Bernhardi *et al.* 2008).

The last term on the right-hand side of eq. (2) represents the current elements **I** at the grid of points. Singular value decomposition technique is used to resolve the system to get the best solution for **I** in the least-squares sense (Amm & Viljanen 1999; McLay & Beggan 2010). Once these currents are obtained, magnetic field variations can be calculated at each point within the grid.

The accuracy of the interpolation can be estimated by the rms between observed and calculated data at a location not used in the inversion:

$$\text{rms} = \sqrt{\frac{1}{n}\sum_{t=1}^{n}\left(B^t_{\text{obs}} - B^t_{\text{SECS}}\right)^2}, \tag{4}$$

where is n the number of samples.

In our model, ionospheric current elements are placed forming two overlapping grids (i.e. 6×6 grid centred at OGA plus a refinement 10×10 grid covering the Uruguayan territory). The mean grid spacing is *ca*. 350 km in the main grid and ∼60 km in the refinement (Fig. 4). Data from three magnetic observatories into the area were used in the interpolation process.

2.2 The ground conductivity model and the geoelectric field

The ground is assumed to be composed of n horizontal layers (Fig. 5), h_i and σ_i being the thickness and conductivity of the

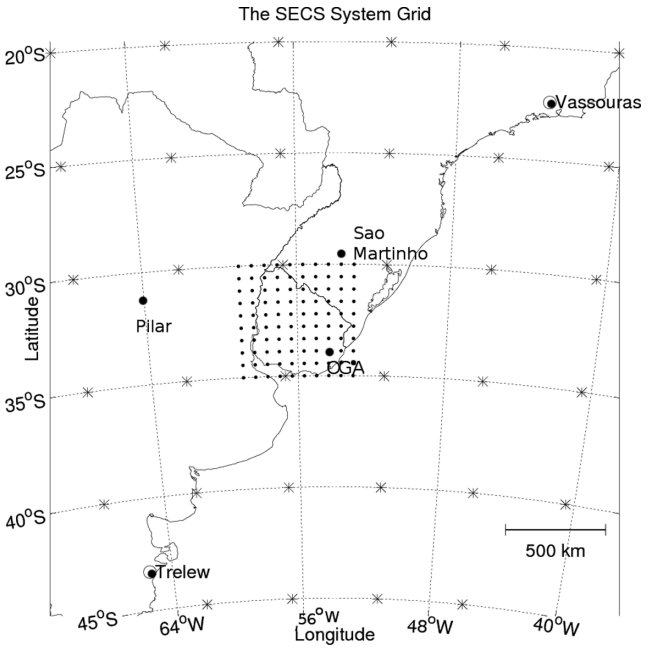

Figure 4. The SECS system used to perform the interpolation showing the refinement grid.

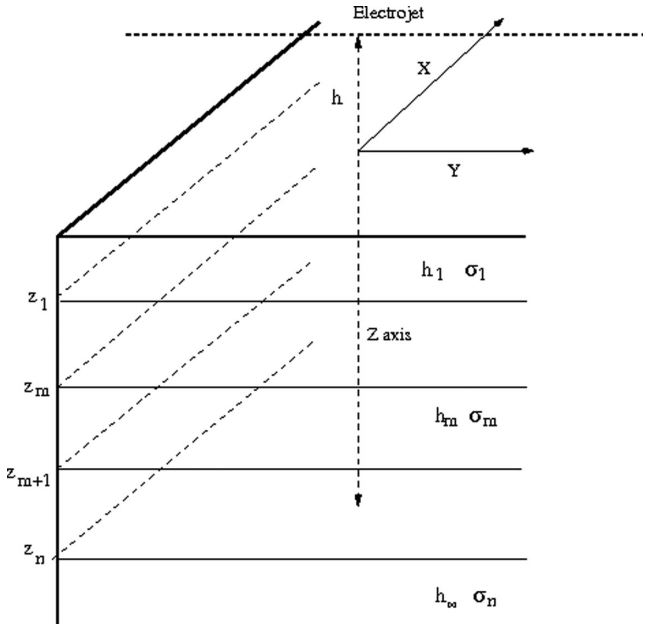

Figure 5. Earth layered model (modified from Zou & Liu 2010).

i-th layer, respectively. Uniform properties are assumed for all layers and the last one is modelled as a semi-infinite half-space downward. The ionospheric current is located at height h above the surface that is considered as the xy-plane of a Cartesian system. The x- and y-axis point northwards and eastwards, respectively, and the z-axis points downwards.

According to the Maxwell equations and the boundary conditions the **E** and **B** fields must satisfy (Pirjola 1982; Zou & Liu 2010), we are led to:

$$\begin{cases} E_{m,x} = C_m e^{-k_m z} + D_m e^{k_m z} \\ B_{m,y} = \frac{k_m}{j\omega}\left(C_m e^{-k_m z} + D_m e^{k_m z}\right), \end{cases} \tag{5}$$

where ω is the frequency and k_m is the wavenumber in the m layer defined as:

$$k_m^2 = j\omega\mu_0\sigma_m, \tag{6}$$

with σ_m representing the m-layer conductivity. Analogous equation system holds for $E_{m,y}$ and $B_{m,x}$ components. Then the wave impedance Z_m in such layer is given by:

$$Z_m = \mu_0 \frac{E_{m,x}}{B_{m,y}}. \tag{7}$$

The C_m and D_m coefficients are defined in such way:

$$r_{m+1} = \frac{D_m}{C_m} = \frac{Z_{m+1} - Z_{0m}}{Z_{m+1} + Z_{0m}} e^{-2k_m z_{m+1}} \tag{8}$$

represent the reflection coefficient at the top of the $(m + 1)$ layer, while Z_{0m} is seen as the wave impedance at the top of an infinitely thick m-layer.

$$Z_{0m} = \frac{j\mu_0\omega}{k_m}. \tag{9}$$

Thus, the wave impedance at the top of the m-layer can be expressed by combining eqs (7)–(9) into a recursive formula:

$$Z_m = Z_{0m} \frac{1 + r_{m+1} e^{-2k_m h_m}}{1 - r_{m+1} e^{-2k_m h_m}}, \tag{10}$$

where h_m is the thickness of the m-layer. Starting from the last layer, eq. (10) gives the surface impedance $Z(\omega)$ (Zou & Liu 2010). The horizontal electric field at the surface is obtained from the horizontal components of the magnetic disturbance as follows:

$$E_{x,y} = \pm \frac{Z(\omega)}{\mu_0} B_{y,x}. \tag{11}$$

2.3 GIC calculation in the power grid

For the second step, the 500 kV grid is modelled as an array of earthed substations from Salto Grande Dam in the North, to San Carlos in the southeast side (Fig. 2). The network has eight points (i.e. substations) and it is mainly north–south oriented. Using Kirchhoff's theorem, we can solve the currents I_{ij} for a network of conductors on the Earth's surface with n earthed nodes linked by resistances R_{ij} $(i, j = 1 \ldots n)$. If there is no connection between the nodes, then R_{ij} is taken as infinite. Let us denote each earthing resistance as r_j, then the current flowing through r_j is I_j. The geovoltage between i and j nodes is given by:

$$V_{ij} = \int_{L_{ij}} \vec{E}.\mathrm{d}\vec{l}. \tag{12}$$

This integral must be performed over the entire path L_{ij} from i to j nodes. The earthing impedance matrix **Z** can be defined as follows: The product of **Z** and a column matrix **I** whose elements are the earthing currents I_j, gives a column matrix where each component is the voltage between the earthing point, and a remote earth associated with the flow of the earthing currents (Pirjola 2007). If the nodes are very far apart, **Z** can be considered as a diagonal matrix where its elements are the earthing resistances.

According to Ohm's law and Kirchhoff's law (Lehtinen & Pirjola 1985) we have:

$$\mathbf{I} = (\mathbf{Id} + \Im\mathbf{Z})^{-1}\mathbf{J}, \tag{13}$$

where **I** is a $N \times 1$ matrix whose elements are the earthing currents at the nodes. **Id** is the unitary identity matrix and $\Im$ is the admittance matrix whose elements are defined by:

$$\Im_{ij} = \begin{cases} -\dfrac{1}{R_{ij}} & i \neq j \\ \displaystyle\sum_{\substack{k=1 \\ i \neq k}}^{n} \frac{1}{R_{ik}} & i = j. \end{cases} \tag{14}$$

J is a column matrix whose elements are defined as:

$$J_i = \sum_{\substack{j=1 \\ j \neq i}}^{n} J_{ji} \quad (i = 1 \ldots n), \tag{15}$$

whose elements represent 'perfect-earthing' (i.e. $\mathbf{Z} = 0$), earthing currents defined as:

$$J_{ji} = \frac{V_{ji}}{R_{ij}}. \tag{16}$$

3 RESULTS AND DISCUSSION

For the interpolation, we start from the minute mean variations of the magnetic field components from Trelew (43.26°S, 65.39°W), Vassouras (22.4°S, 43.6°W) and São Martinho da Serra (29.43°S,

53.8°W) magnetic observatories, registered on 2003 October 29. Baseline values were removed from all data sets to get the *X*, *Y* variations and then used as input for the SECS algorithm.

Horizontal magnetic field components are converted from time domain to frequency domain, the surface impedance *Z* is derived according eq. (10). Then, the results are transformed back to the time domain to give the **E** components.

Regarding the ground conductivity, it is necessary to know the geology of the Uruguayan region. According to Sánchez Bettucci *et al.* (2010), the units that constitute the country are a Precambrian basement, to the west, composed by Piedra Alta and Nico Pérez tectonostratigraphic terranes, separated by the Sarandí del Yí Shear Zone. The Piedra Alta tectonostratigraphic terrane includes low to medium metamorphic orogenic belts (*ca.* 2.1 Ga), layered mafic complex, late- to post-orogenic magmatism(1.9–2.3 Ga), rapakivi granites (2.078 Ga) and mafic dyke swarm (1.7 Ga). The Nico Pérez terrane is constituted fundamentally by granitoids and partially affected by the Brasiliano–Pan African orogenic cycle (Neoproterozoic). This last orogenic cycle is represented in Uruguay and southern Brazil by the Dom Feliciano Belt that developed between *ca.* 750 and 550 Ma and comprise metavolcanosedimentary rocks and some gabbros intrusions. The metasedimentary sequence contains metapelites, metapsamites and marbles. The Phanerozoic units are mainly located at the north and west of Uruguay. The units are Paraná foreland basin developed through the Palaeozoic to Cenozoic, Mesozoic bimodal volcanism and large igneous provinces, rift deposits and intracratonic basin (Rapalini & Sánchez Bettucci 2008; Sánchez Bettucci *et al.* 2010, see Fig. 6).

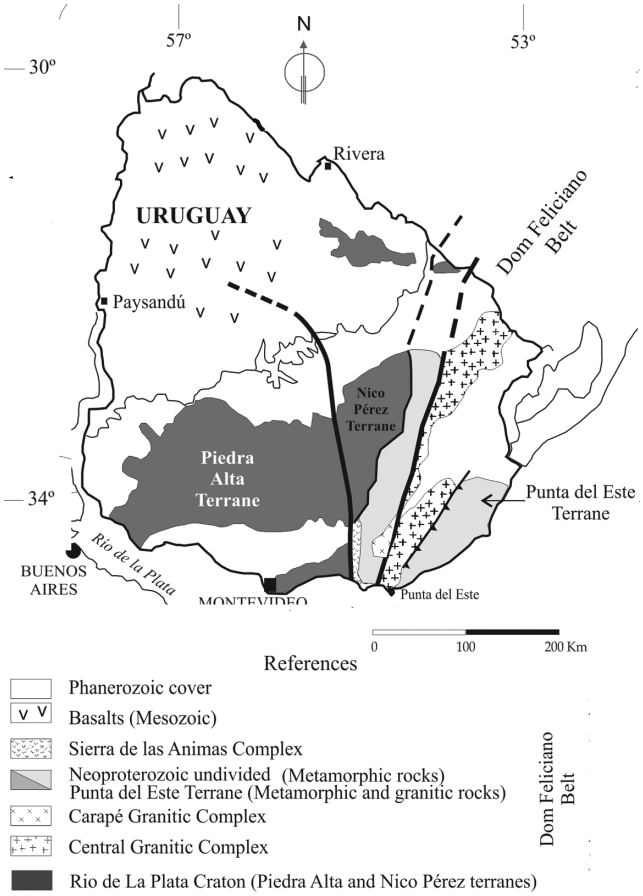

Figure 6. Geological sketch of the Uruguayan territory (modified from Rapalini & Sánchez Bettucci 2008).

Table 1. Layered earth profile parameters.

Profile 1		Profile 2	
Thickness (km)	Conductivity (Sm^{-1})	Thickness (km)	Conductivity (Sm^{-1})
0–1.5	0.003	0–0.5	0.0067
1.5–3	0.05	0.5–100	0.001
3–100	0.001	>100	0.1
>100	0.1		

Ground conductivity available studies cover a small area in the north of the Uruguayan territory. Gravimetric surveys suggest a litospheric crust thickness *ca*. 116 km deep (Introcaso & Huerta 1982) Two unidimensional ground conductivity profiles were inferred on the basis of magnetotelluric transects performed along the NW border. A four horizontal layer model was used covering the Phanerozoic units at the NW of the country and a three horizontal layer model for the Precambrian units at the SE of the country (Introcaso & Huerta 1982; Sánchez Bettucci *et al.* 2010). The thicknesses and conductivities in each layer are showed in Table 1.

Regarding the network parameters, a common value of 0.7 Ω was chosen for all earthing impedances. These earthing impedances are the sum of the transformer resistances and the actual earthing resistances. It was difficult to obtain detailed network parameters from the electricity company. A mean conductor resistivity of 0.035 Ω km^{-1} was used, reducing all the three phases to a single line. Network parameters were suggested considering the official documentation available or by direct inspection. GIC calculation was focused between Salto Grande–San Javier (140 km) and Palmar–Montevideo (220 km) sections (Fig. 2), which are mainly N–S and NW–SE oriented, respectively. The Salto Grande–San Javier section is localized over the Chaco–Parana basin (Corbo *et al.* 2012), while the Palmar–Montevideo section is situated over the Piedra Alta outcrop (Fig. 5). If the **E** field is quite uniform between two close points, the eq. (12) for the geovoltage can be approximated by:

$$V_{ij} = L_{ij}(E_x \sin\theta + E_y \cos\theta), \tag{17}$$

where L_{ij} and θ are the linear distance between points *i* and *j* and the angle between the L_{ij} linear path and the *y*-axis (i.e. eastward direction), respectively.

Due to its dc-like nature, GIC over the secondary branches was neglected. These branches usually connect through the secondary windings at the HV transformers, and not all secondary branches are interconnected to the considered network.

The graph of the variations of the *X*, *Y* components at OGA (Fig. 7b) suggest rates of change up to ±90 nT min^{-1} particularly in the *X* component for the event considered. The two last plots in the same figure show the electric field components (E_x, E_y), calculated by eq. (11) from the geomagnetic data. Notable differences are seen between the two graphs, particularly E_y variations results to be more prominent than E_x ones. However, there are considerable variations in E_y component around 6:00 and 14:00 hr UTC showing several peak values *ca.* 1 V km^{-1}. The first of these, near 6:00 hr can be related to the storm commencement.

Further calculation along the 10 × 10 grid revealed a quasi-uniform spatial distribution for the geoelectric field over the main geological units along the Uruguayan territory. Field values becomes more intense along the southern part of the territory, due to the increase in the ground impedance. Also it is expected some distortion along the border between the two ground types. This feature can be ascribed to the simplicity of the ground models. Fig. 8

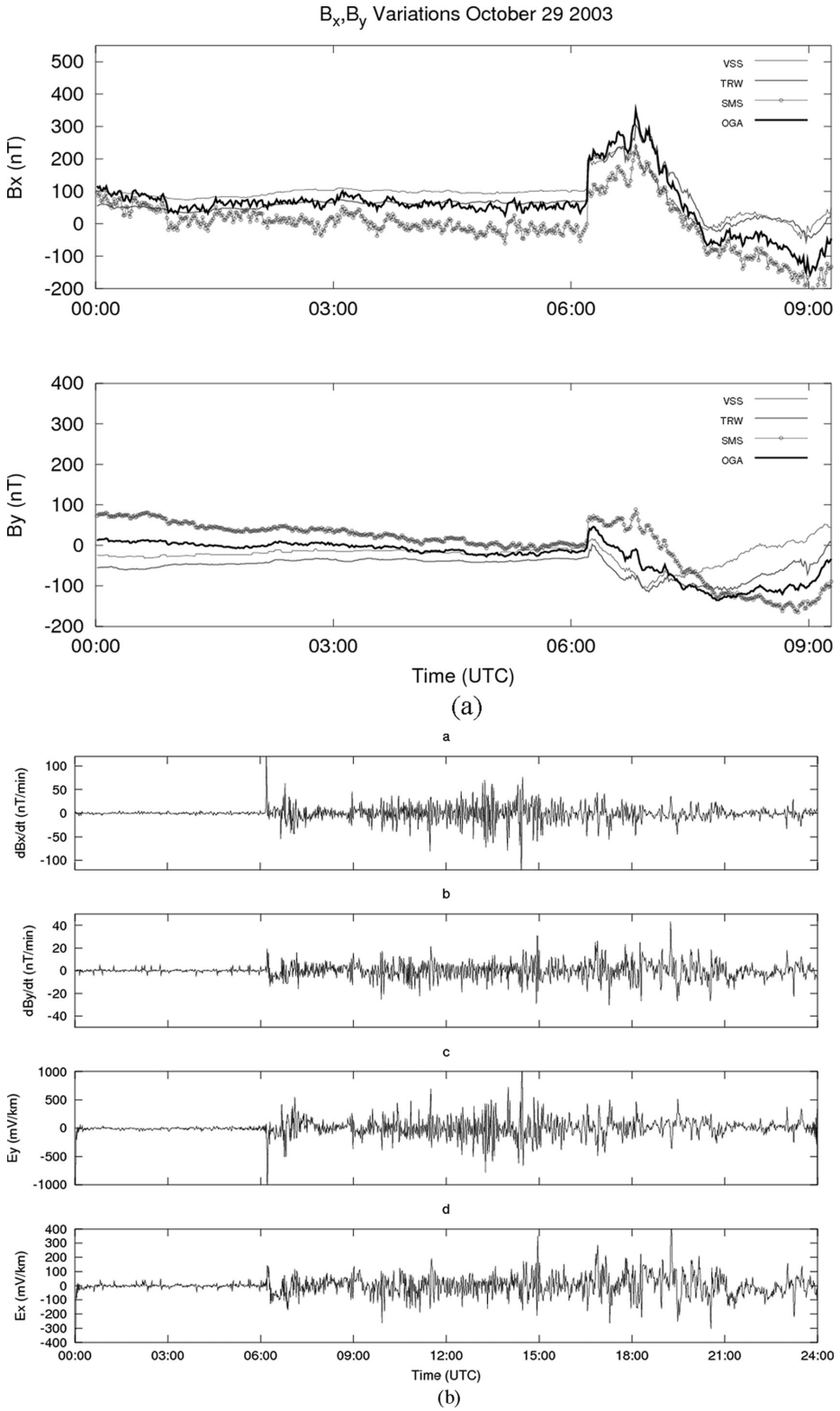

Figure 7. (a) Geomagnetic field interpolated at OGA (bold line) versus values registered at Vassouras (VSS), Trelew (TRW) and São Martinho da Serra (SMS) stations. (b) Variations of the horizontal geomagnetic components interpolated at OGA (a, b). Horizontal electric field components calculated from *X* and *Y* data at the same site (c, d). (c) Top panel: Comparison between registered and interpolated variations at PILAR (PIL) station, with the values registered at Vassouras (VSS), and Trelew (TRW) for the great storm on 1958 February 2. Lower panel: In a similar way, but at São Martinho station for the Halloween storm in 2003.

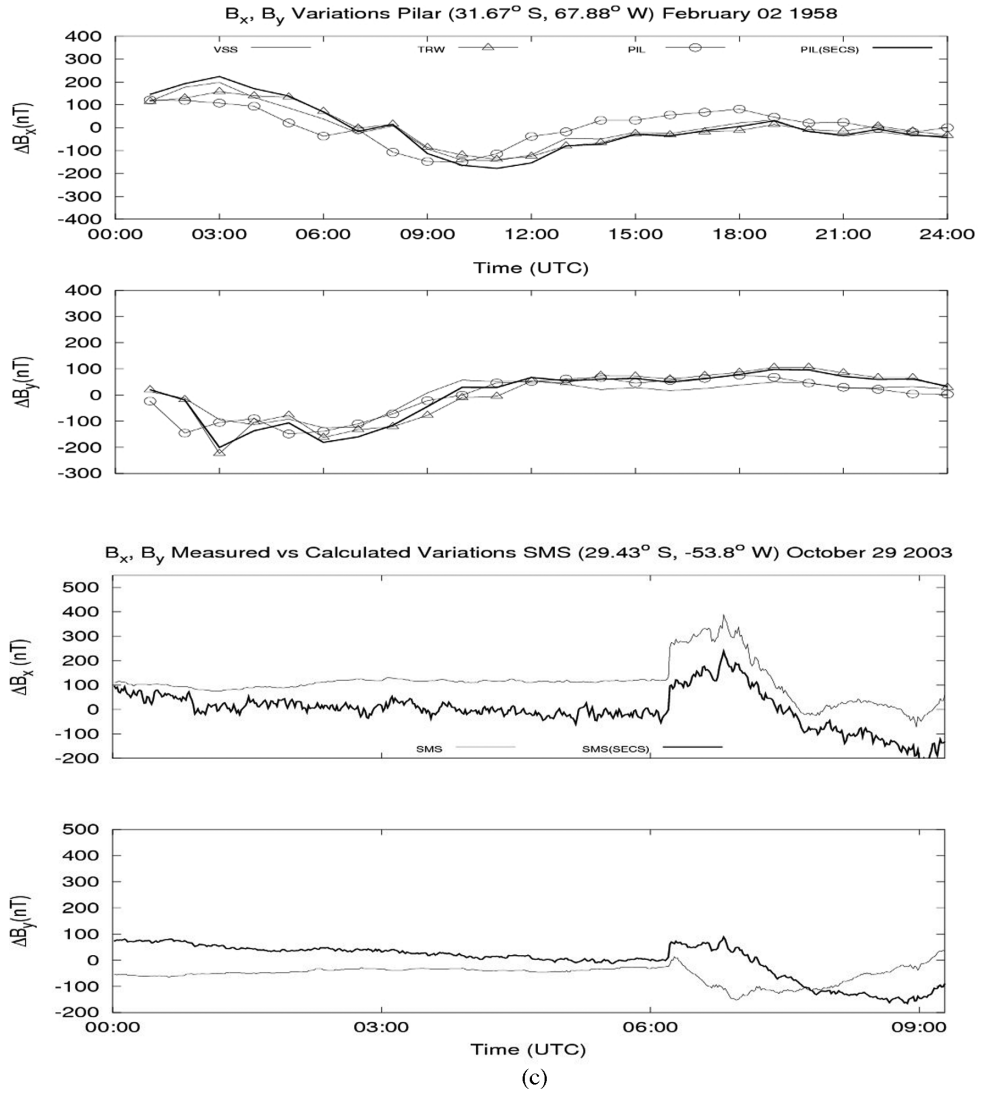

(c)

Figure 7. (*Continued.*)

shows a vector plot of the geoelectric field at 6:10 hr during the storm's onset.

Some criticism is needed due to the interpolation considered to perform the GIC modelling, especially with scarce and spread number of observations. At this point, we follow a similar treatment as in the work of McLay & Beggan (2010). Because there is lack of geomagnetic records in the Uruguayan territory, interpolation parameters were previously tested with observations made at São Martinho (SMS) and Pilar magnetic stations, 700 and 550 km away, respectively (Fig. 1).

The closest similar events registered simultaneously by Vassouras and Trelew stations were the great storm on 1958 February 2 (Dst −426 nT) and the storm on 2003 October 29 (Dst $\sim$ −400 nT), where the Dst index is a measure of the storm intensity, the more negative value, more severe is the storm. Both events were chosen to make the comparison. The available Pilar data consist in hourly means: the first two panels in Fig. 7(c) show a (rough) comparison between the *X* and *Y* components registered and interpolated there. The lower two panels show the same comparison for São Martinho station (SMS) on 2003 October 29. SMS plots exhibit more details due to the use of minute means in this case.

Table 2 shows the rms (or misfit) calculated in both comparisons.

In both cases, SECS yields a better estimation for the *Y* component than the *X* one. This feature agrees with the fact that the field varies more quickly in the North–South direction. In a similar way, the misfit (rms) between interpolated components at OGA station, including and excluding SMS data, gives 67.25 nT and 52 nT for the *X* and *Y* components, respectively. Data provided by the São Martinho magnetic station improved the results (Fig. 7a). However, the interpolation gives still reasonable results, if only the two distant observation sites are considered. This fact suggests a longitudinal uniformity in the magnetic field variations across the area, which makes the interpolation reliable, even in a spatial scale greater than 600 km in the E–W direction (Ngwira *et al.* 2009).

The Halloween magnetic storm in 2003 had unique characteristics (Kappenman 2005), and is one of the top 10 greater storms in the last 50 yr. The variations calculated show similarities with those reported by Bernhardi *et al.* (2008) and Kappenman (2005).

The eq. (17) was used to calculate the potential difference between nodes in the network. Fig. 9 shows the estimated GIC flowing at the earthing points of two particular substations. In both graphs we see significant values in the GIC at 06:00 and 14:00 hr UTC, respectively, followed by minor variations. The intensity peaks last

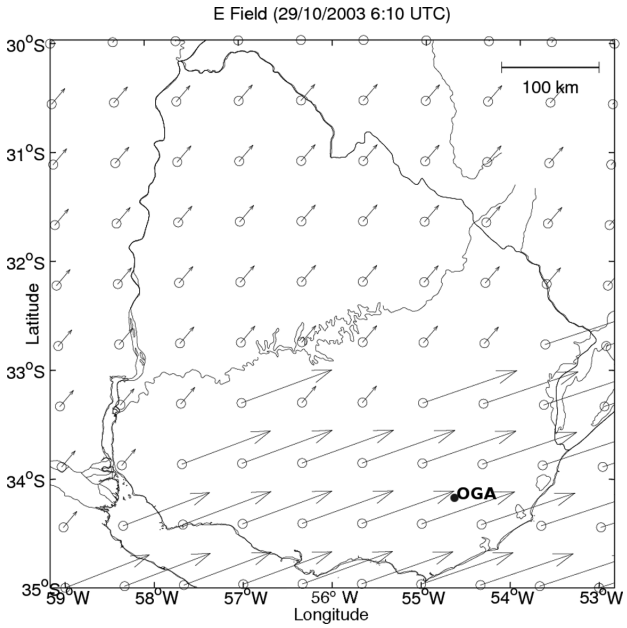

Figure 8. Horizontal electric field over the Uruguayan territory at the storm onset, 2003 October 29 (6:10 UTC).

Table 2. rms values at Pilar (PIL) and São Martinho(SMS) sites.

Component	(PIL) (nT)	(SMS) (nT)
X	73.58	116.2
Y	45.76	89.2

several minutes in each case. We get also larger values in the GIC for the Salto Grande–San Javier section despite its shorter length.

Calculated GIC values are similar to those reported in some sections of the Brazilian power grid, for the magnetic storm on 2004 November 7–10 (Dst −383 nT) and South Africa on 2003 October 30 (Trivedi *et al.* 2007; Bernhardi *et al.* 2008).

Regarding the Uruguayan geological ground characteristics, the existence of shallow high-resistivity layers may contribute to increased GIC intensity in some sections. The power grid geometry and the fact of a quite uniform geoelectric field make the calculation easier. Some differences are expected by factors like transversal non-uniform ground conductivity and charge accumulation at coastal areas (Molinski 2002). In these regions, the induced currents flowing in the ocean meet a higher resistance as they enter in the land (Kappenman 2007). Moreover, we have considered similar earthing resistances for all substations. Uruguayan power utilities obey the ANSI/IEEE 80 standards that recommend a maximum earthing resistance of 1 Ω for the HV substations. Then, in the worst case, if these resistances vary to some extent, a moderated variation in the GIC should be expected.

The impulsive disturbances in the geomagnetic field near 7:00 UTC (Figs 7a and b), correlate well with the arrival of solar wind pressure pulses at the leading edge of the coronal mass ejection (CME). In both cases, interpolated data agree with the characteristic features of the 2003 October 28–31 storm. Long-period impulses in the horizontal geomagnetic field components associated with high variation rates have been pointed as the source of GIC. These phenomena are ascribed to compressions of the magnetosphere by high speed solar wind ($\sim$2000 km s^{-1}) (NOAA 2004). The pulsations are considered as a consequence of the Kelvin–Helmholtz shear process (Russell 2000; Kappenman 2005). With respect to the particle fluxes influence, Fig. 10 shows the electron flux with energy $\geq$2 MeV and a frequency analysis of the flux variation registered by GOES 12 (75°W) satellite over South America. We can see again a large peak near the 6:00 UTC and a subsequent nearly monotonic decay in the particle fluxes. The decay may be explained as a consequence of electron pitch angle diffusion into the atmosphere. This feature agrees with similar plot of X-Ray flux (NOAA, 2004) and the frequency analysis shows small pulses in the period

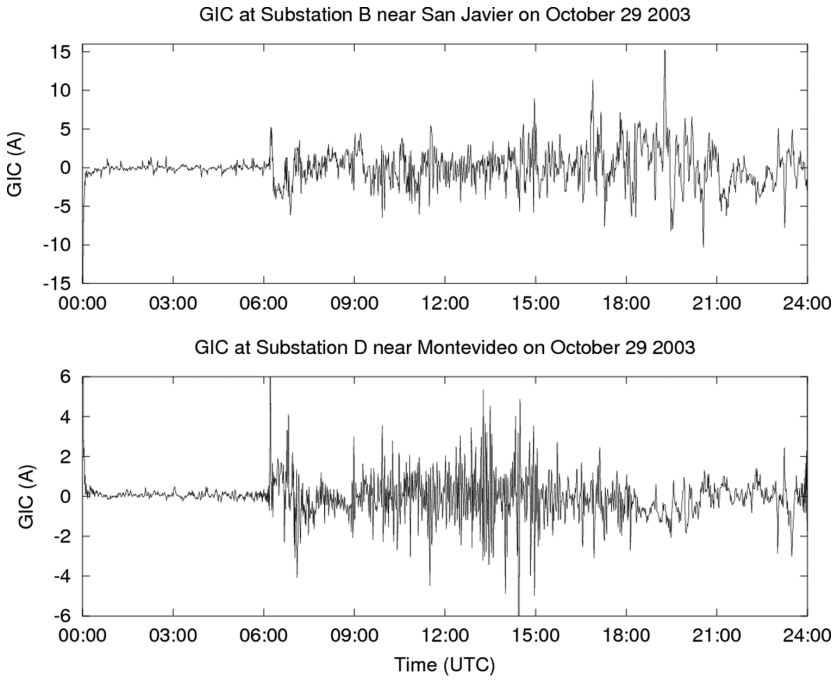

Figure 9. Calculated GIC through transformer's neutral at two substations: San Javier (top panel) and Montevideo (lower panel) during the magnetic storm on 2003 October 29.

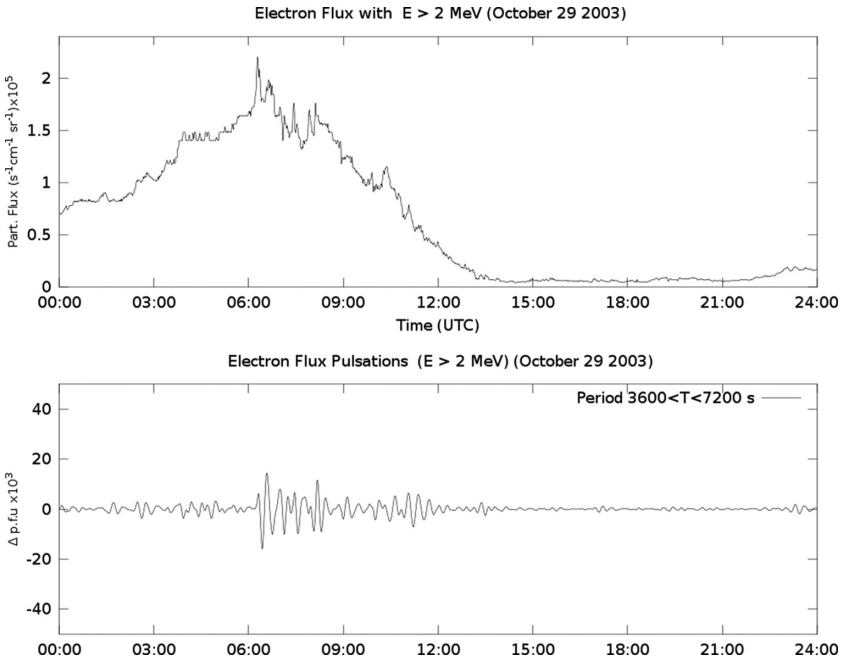

Figure 10. Electron flux with $E \geq 2$ MeV (top panel) and its filtered variations in the period range 3600–7200 s (bottom panel), registered by GOES 12 satellite (2003 October 29).

range of 3600–7200 s close to the storm commencement. In both cases, large impulses have been observed in GIC and electron fluxes near 6:00 hr, with secondary peaks at 15:00 hr and 21:00 hr UTC. Similar behaviour is observed in magnetic registers provided by the three magnetic stations.

4 CONCLUSIONS

We estimated GIC currents over a mid-latitude power grid for the Halloween magnetic storm that caused serious failures in the South African power network. GIC calculations suggest quite similar temporal variations as those reported by Bernhardi *et al.* (2008) and Ngwira *et al.* (2009) Interpolation results show similar geomagnetic variations in the whole area despite the few points of observation available. The South American region has few and spread magnetic observatories, almost all at the external part of the SAA. It is expected that GIC effects could be similar, or even more intense over the larger power grids of Brazil and Argentina. South Africa lies around the same latitude as Uruguayan territory, considering the intensity of GIC reported in Brazilian (Trivedi *et al.* 2007) and in South African (Bernhardi *et al.* 2008; Ngwira *et al.* 2009) power lines. Thus, the calculated values for GIC can be considered in fair agreement with the actual figures.

According to this, GIC phenomenon may represent a potential threat to power utilities in South America, specially the longer ones. Further studies are necessary to characterize the actual impact of GICs over the technological infrastructure in this area. Future studies will have to improve the ground conductivity models and grid parameters to get a more accurate assessment of GIC phenomena. Unfortunately, it was not possible to obtain failure records of the Electricity Company during that time. Some power industry operators in South American countries are not entirely aware of GIC phenomena. This fact increases the risk of catastrophic failures in power lines due to the lack of mitigation measures.

The 2003 October 29 magnetic storm proved that GICs are relevant even in low to mid-latitudes, and may cause damages in power grids (Trivedi *et al.* 2007; Bernhardi *et al.* 2008). It is important to monitor the ionospheric currents and particle fluxes over the SAA and its impact on GIC production in power utilities, communication systems, among others. It would be very helpful to get more direct measurements of GIC in power grids and pipelines to improve accuracy. Then, we consider justified the installation of a new magnetic observatory in the Uruguayan territory. The new observatory facilities will provide a continuous register of the geomagnetic field variability over the Rio de la Plata region 24 hr a day.

ACKNOWLEDGEMENTS

The authors thank the referees for their comments that helped to clarify the presentation. Special thanks to Dr N. Schuch who provided useful data from São Martinho da Serra Observatory. Also thanks to Profs V. Baratelli and W. Gomez for their revision of the English manuscript. All the data used in this paper were supplied freely by the NOAA National Geophysical Data Center, the U.S, Geological Survey and the British Geological Survey.

REFERENCES

Amm, O. & Viljanen, A., 1999, Ionospheric disturbance magnetic field continuation from the ground to the ionosphere using spherical elementary current systems, *Earth Planets Space,* **51,** 431–440

Bernhardi, E.H., Cilliers, P.J. & Gaunt, C.T., 2008. Improvement in the modelling of geomagnetically induced currents in southern Africa, *S. Afr. J. Sci.,* **104**(7–8), 265–272.

Boteler, D.H. & Pirjola, R., 1998. Modelling geomagnetically induced currents produced by realistic and uniform electric fields, *IEEE Trans. Power Del.,* **13**(4), 1303–1308.

Corbo, F., Arzate, J. & Oleaga, A., 2012. Structure of the Guarani aquifer in the surroundings of the Uruguay river from magnetotelluric soundings, *Geofisica Internacional,* **51,** 17–37.

Introcaso, A. & Huerta, E., 1982. Interpretación del exceso de gravedad en Uruguay, *5° Congreso Latinoamericano de Geología,* Actas 4: 87-104, Buenos Aires, Argentina.

Jayanthi, U.B., Pereira, M.G., Martin, I.M., Trivedi, N.B. & Lazutin, L., 1997. X-Ray Observations in the SAA-pulsations in electron precipitation accompanied by Pc4 events, *Adv. Space Res.,* **20**(3), 509–512.

Kappenman, J.G., 2007. Geomagnetic disturbances and impacts upon power system operation, in *The Electric Power Engineering Handbook,* 2nd edn, Ch. 16, pp. 1–22, ed. Grigsby, L.L., CRC Press/IEEE Press.

Kappenman, J.G., 2005. An overview of the impulsive geomagnetic field disturbances and power grid impacts associated with the violent Sun-Earth connection events of 29–31 October 2003 and a comparative evaluation with other contemporary storms, *Space Weather,* **3,** S08C01, doi:10.1029/2004SW000128.

Kivelson, M.G. & Russell, C.T., 1995. *Introduction to Space Physics,* Cambridge University Press.

Lehtinen, M. & Pirjola, R., 1985. Currents produced in earthed conductor networks by geomagnetically-induced electric fields, *Ann. Geophys.,* **3,** 479–484.

McLay, S.A. & Beggan, C.D., 2010. Interpolation of externally-caused magnetic fields over large sparse arrays using Spherical Elementary Current Systems. *Ann. Geophys.,* **28,** 1795–1805.

Molinski, T.S., 2002. Why utilities respect geomagnetically induced currents, *J. Atmos. Sol. Terr. Phys.,* **64,** 1765–1778.

National Oceanic and Atmospheric Administration (NOAA), 2004. *Halloween space weather storms of 2003. Tech Memo, OAR SEC-88,* Silver Spring, MD.

Ngwira, C.M., McKinnell, L.-A., Cilliers, P.J., Viljanen, A. & Pirjola, R., 2009. Limitations of the modeling of geomagnetically induced currents in the South African power network, *Space Weather,* **7,** S10002, doi:10.1029/2009SW000478.

Pirjola, R., 1982. Electromagnetic induction in the earth by a plane wave or by fields of line currents harmonic in time and space, *Geophysica,* **18,** 1–161.

Pirjola, R., 2007. Calculation of geomagnetically induced currents (GIC) in a high-voltage electric power transmission system and estimation of effects of overhead shield wires on GIC modelling, *J. Atmos. Sol. Terr. Phys.,* **69**(12), 1305–1311.

Rapalini, A.E. & Sánchez Bettucci, L., 2008. Geomagnetism, rock magnetism and palaeomagnetism widespread remagnetization of late Proterozoic sedimentary units of Uruguay and the apparent polar wander path for the Rio de La Plata craton, *Geophys. J. Int.,* **174,** 55–74.

Russell, C.T., 2000. The solar wind interaction with the earth's magnetosphere: a tutorial, *IEEE Tran. Power Del.,* **28**(6), 1818–1830.

Sánchez Bettucci, L., Peel, E. & Oyhantçabal, P., 2010. Precambrian geotectonic units of the Río de La Plata Craton, *Int. Geol. Rev.,* **52**(1), 32–50.

Trivedi, N.B., Pathan, B.M., Schuch, Nelson J., Barreto, M. & Dutra, L.G., 2005. Geomagnetic phenomena in the South Atlantic anomaly region in Brazil, *Adv. Space Res.,* **36,** 2021–2024.

Trivedi, N.B. *et al.*, 2007. Geomagnetically induced currents in an electric power transmission system at low latitudes in Brazil: a case study, *Space Weather,* **5,** S04004, doi:10.1029/2006SW000282.

Zou, M. & Liu, L., 2010. GIC calculation in power grid based on layered earth mode, in *Proceedings of 2010 5th International Conference on Critical Infrastructure (CRIS),* pp. 1 and 4, 20–22 September 2010, Beijing, China.